Co-localization of two-color rAAV2-retro confirms the dispersion characteristics of efferent projections of mitral cells in mouse accessory olfactory bulb

ZOOLOGICAL RESEARCH

Co-localization of two-color rAAV2-retro confirms the dispersion characteristics of efferent projections of mitral cells in mouse accessory olfactory bulb

Ning Zheng[1,2,#], Zhi-Zhong Wang[3,#], Song-Wei Wang[3,#], Fang-Jia Yang[4], Xu-Tao Zhu[1], Chen Lu[4], Anne Manyande[5], Xiao-Ping Rao[1,*], Fu-Qiang Xu[1,2,6,*]

[1] *Center of Brain Science*, *State Key Laboratory of Magnetic Resonance and Atomic and Molecular Physics*, *National Center for Magnetic Resonance in Wuhan*, *Key Laboratory of Magnetic Resonance in Biological Systems*, *Wuhan Institute of Physics and Mathematics*, *Innovation Academy for Precision Measurement Science and Technology*, *Chinese Academy of Sciences*, *Wuhan*, *Hubei* 430071, *China*

[2] *University of the Chinese Academy of Sciences*, *Beijing* 100049, *China*

[3] *Department of Automation*, *School of Electrical Engineering*, *Zhengzhou University*, *Zhengzhou*, *Henan* 450001, *China*

[4] *School of Life Science*, *Wuhan University*, *Wuhan*, *Hubei* 430072, *China*

[5] *School of Human and Social Sciences*, *University of West London*, *Middlesex*, *TW89GA*, *UK*

[6] *Divisions of Biomedical Photonics*, *Wuhan National Laboratory for Optoelectronics*, *Wuhan*, *Hubei* 430074, *China*

ABSTRACT

The accessory olfactory bulb (AOB), located at the posterior dorsal aspect of the main olfactory bulb (MOB), is the first brain relay of the accessory olfactory system (AOS), which can parallelly detect and process volatile and nonvolatile social chemosignals and mediate different sexual and social behaviors with the main olfactory system (MOS). However, due to its anatomical location and absence of specific markers, there is a lack of research on the internal and external neural circuits of the AOB. This issue was addressed by single-color labeling and fluorescent double labeling using retrograde rAAVs injected into the bed nucleus of the stria terminalis (BST), anterior cortical amygdalar area (ACo), medial amygdaloid nucleus (MeA), and posteromedial cortical amygdaloid area (PMCo) in mice. We demonstrated the effectiveness of this AOB projection neuron labeling method and showed that the mitral cells of the AOB exhibited efferent projection dispersion characteristics similar to those of the MOB. Moreover, there were significant differences in the number of neurons projected to different brain regions, which indicated that each mitral cell in the AOB could project to a different number of neurons in different cortices. These results provide a circuitry basis to help understand the mechanism by which pheromone information is encoded and decoded in the AOS.

Keywords: Accessory olfactory bulb; Efferent projections; Retrograde rAAVs; Projection neuron labeling; Dispersion characteristics; Circuitry basis

Received: 18 September 2019; Accepted: 25 December 2019; Online: 31 December 2019

Foundation items: This work was supported by the Natural National Science Foundation of China (31400946, 31771156, 91632303/H09, 91732304 and 31830035) and Strategic Priority Research Program of the Chinese Academy of Sciences (XDB32030200)

#Authors contributed equally to this work

*Corresponding authors, E-mail: raoxiaoping0902@wipm.ac.cn; fuqiang.xu@wipm.ac.cn

DOI: 10.24272/j.issn.2095-8137.2020.020

INTRODUCTION

Most animals rely heavily on their chemosensory perception to interact with their surroundings, with a variety of odor molecules carrying a wealth of information. Chemical senses, based on the detection of molecules, trigger physiological, reproductive, and social responses, and play essential roles in foraging and avoidance, escaping from predators, and locating suitable mating partners (Su et al., 2009). Terrestrial vertebrates have two anatomically distinct and functionally overlapping (in part) olfactory systems: i.e., the main olfactory system (MOS) and accessory olfactory system (AOS), which can, in parallel, detect and process volatile and nonvolatile social chemosignals and mediate different sexual and social behaviors through different receptors and signal transduction pathways (Spehr et al., 2006). The AOS is a relatively "simple" combination of neural circuits with complex information processing mechanisms and is directly related to neuroendocrine changes, emotional changes, and social/sexual behaviors, making it an ideal model for studying chemical sensory coding (Mohrhardt et al., 2018).

The vomeronasal organ (VNO), which comprises the peripheral sensory structure of the AOS, plays a major role in detecting both hetero- and con-specific social cues that convey information about identity, gender, social rank, and sexual state (Ackels et al., 2016). The VNO is a bilaterally symmetrical, cylindrical organ encased in a bony capsule on the anterior nasal septum. It is blind posteriorly with a crescent-shaped sensory epithelium located at the medial wall of the organ and a large blood vessel running laterally to the lumen. Furthermore, depending on the species, it opens anteriorly into either the nasal or oral cavity to allow entry of chemosignals, especially nonvolatile chemical cues, after direct physical contact of the snout with odor sources (Doving & Trotier, 1998; Dulac & Torello, 2003; Halpern & Martinez-Marcos, 2003). Within the VNO, sensory neurons can be categorized into two segregated subpopulations organized in separate layers of the vomeronasal epithelium. Cells expressing type-I vomeronasal receptors (V1Rs) or formyl peptide receptors (FPRs) and Gi proteins in the apical layer project to the anterior part of the accessory bulb (aAOB). However, cells in the basal layer expressing type-II vomeronasal receptors (V2Rs) and Go proteins project to the posterior part of the AOB (pAOB) (Dulac & Torello, 2003; Riviere et al., 2009). The V1R/FPR-expressing cells are responsive to small hydrophobic molecules, such as volatile urinary components or pathogenic molecules emitted by sick animals (Leinders-Zufall et al., 2000; Riviere et al., 2009). The sensory neurons expressing V2Rs, which contain a large N-terminal domain and form ligand binding sites, respond to proteinaceous components (Breer et al., 2006; Krieger et al., 1999; Leinders-Zufall et al., 2004).

The AOB, located at the posterior dorsal aspect of the main olfactory bulb (MOB), is the first brain relay of the AOS and has a compact laminar structure approximately 1.5 mm (anterior-posterior) by 0.6 mm (medial-lateral) in surface area (Holy, 2018). The AOB shares many similarities with the larger MOB in broad classes of neuronal populations, layered organization, and connectivity. Yet, the AOB and MOB also show notable differences with respect to cytoarchitecture, glomerular formation, and physiological and morphological properties of projection neurons (Dulac & Wagner, 2006; Larriva-Sahd, 2008; Mohrhardt et al., 2018; Moriya-Ito et al., 2013; Urban & Castro, 2005; Yokosuka, 2012; Yoles-Frenkel et al., 2018; Yonekura & Yokoi, 2008). Each mitral cell contains multiple thick glomerular (or primary) dendrites toward multiple glomeruli (ranging between 2 and 10) (Takami & Graziadei, 1991; Urban & Castro, 2005; Yonekura & Yokoi, 2008). This unique organization is markedly distinct from that in the MOB, where each mitral cell contacts a single glomerulus (Su et al., 2009). Moreover, the thin secondary (accessory) dendrites, emanating from the cell body, are shorter and fewer in number than in the MOB mitral cells (Mohrhardt et al., 2018).

However, due to its anatomical location and absence of specific markers, there is a lack of research on the internal and external neural circuits of the AOB. For example, projection of the MOB is characterized by one-to-many, that is, the axonal branches of individual mitral cells can reach all olfactory cortices (Nagayama et al., 2010). This indicates that the encoded and transmitted odor information may be similar, but different olfactory cortices may have different odor decoding mechanisms, which eventually lead to the perception of odorants. The question is, does the AOB have similar projection characteristics as the MOB? Although the fine structure and configuration of these projections have been investigated in the MOB (Ghosh et al., 2011; Miyamichi et al., 2011; Nagayama et al., 2010; Sosulski et al., 2011), the projection characteristics of mitral cells in the AOB remain unknown.

In the present study, we successfully infected the mitral cell layer of the AOB (MiA) with rAAV2-retro absorbed by their terminal axons in different accessory olfactory cortices, including the bed nucleus of the stria terminalis (BST), anterior cortical amygdalar area (ACo), medial amygdaloid nucleus (MeA), and posteromedial cortical amygdaloid area (PMCo), thus indicating the effectiveness of this method for AOB projection neuron labeling. We then used two-color rAAV2-retro to achieve the co-labeling of mitral cells in the AOB from two different cortices. Results showed that the projection patterns of mitral cells in the AOB were like those of the MOB. Hence, the decoding mechanism of pheromones in the AOS may be similar to that in the MOS. Moreover, there may be significant differences in the number of neurons projected to the same area in different brain regions, indicating that each mitral cell in the AOB could project to a different number of neurons in different cortices.

MATERIALS AND METHODS

Animals

All surgical and experimental procedures were conducted in accordance with the guidelines of the Animal Care and Use

Committees at the Wuhan Institute of Physics and Mathematics, Chinese Academy of Sciences (reference No.: WIPM-(2014)39). Adult male C57BL/6 mice (15–40 weeks old, purchased from Hunan SJA Laboratory Animal Company, China) were housed in a specific pathogen-free facility under a controlled room temperature (22±2 °C), humidity (60%–80%), and 12 h:12 h light/dark cycle. Food and water were available *ad libitum*.

Virus injection

Recombinant rAAV2-retro-Ef1α-EYFP-WPRE-pA and rAAV2-retro-Ef1α -mCherry-WPRE-pA were prepared by BrainVTA (China). Animals were anesthetized with chloral hydrate (400 mg/kg), and then placed in a stereotaxic apparatus (RWD, China). During surgery and virus injection, anesthesia was maintained with isoflurane (1%). The skull above the target areas was thinned with a dental drill and removed carefully. Injections were administered with a syringe pump (Quintessential Stereotaxic Injector, USA) connected to a glass micropipette with a tip diameter of 10–15 mm. rAAV2-retro (80 nL, 1×10^{13} vg/mL) was injected (8 nL/min) respectively into the accessory olfactory cortex of adult C57 mice with the following coordinates: BST (AP, 0 mm; ML, –0.6 mm; DV, –4.5 mm), ACo (AP, –0.58 mm; ML, –2.35 mm; DV, –5.7 mm), MeA (AP, –1.1 mm; ML, –2.0 mm; DV, –5.0 mm), PMCo (AP, –3.08 mm; ML, –3.2 mm; DV, –5.25 mm). Four weeks after virus infection, the animals were transcardially perfused with physiological saline followed by 4% paraformaldehyde (PFA).

Tissue section preparation, imaging, and data analysis

Brains were removed, post-fixed in PFA overnight, and dehydrated in 30% (w/v) sucrose for 3 d. The AOB was sagittally sectioned and the accessory olfactory cortex was coronally sectioned on a cryostat microtome (NX50, Thermo, USA). Sequential whole-brain sections (50 μm thick) were transferred into antifreeze solution (50% PBS, 30% ethylene glycol, 20% glycerol) in 24-well plates for storage at −25 °C. For fluorescent imaging, they were wet-mounted with DAPI, sealed with nail polish, and imaged with the VS120 virtual microscopy slide-scanning system (Olympus, Japan). All slices of the AOB were photographed and the number of labeled cells was counted, with the posterior cortex sampled at intervals of 300 μm. The acquired images were processed with Adobe Photoshop CS4 and Adobe Illustrator CS6.0 for illustrations. For cell counting in ImageJ, the boundaries of brain regions were delineated manually based on the Allen Brain Atlas and Mouse Brain Atlas (Fourth Edition) and the labeled neurons were quantified by the cell counter plug-in. For all statistical analyses in SPSS (v13.0), we first verified that all data were normally distributed using the one-sample Kolmogorov-Smirnov test, then calculated the mean value, standard deviation, and standard error of each group, with one-way ANOVA followed by *post-hoc* test used to determine statistical differences between groups. Statistical significance was set at $P<0.001$, $P<0.01$, and $P<0.05$. Numbers of labeled neurons and co-labeling percentages were presented as means±*SD* and means±*SEM*, respectively. Graphs were made using GraphPad Prism (v7.0).

RESULTS

AOB projects to BST, ACo, MeA, and PMCo

To verify the effectiveness of labeling the mitral cells of the AOB, we injected retrograde tracers into different accessory olfactory cortices of mice. The primary data showed that the MiA could be labeled by cholera toxin B (CTB, not shown) or by rAAV2-retro injected in the BST, ACo, MeA, and PMCo (Figure 1A–H). These results indicated that the AOB could project to the BST, ACo, MeA, and PMCo. In addition, we found that the number of infected neurons in the MiA per slice varied in different retrograde-labeled brain regions (Figure 1I). Among them, the infected neurons were greatest in MeA and PMCo labeling (MeA: 111.06±74.39, PMCo: 117.12±82.213), followed by ACo labeling (ACo: 48.3±36.943), and finally BST labeling (BST: 26.05±20.061), with significant differences found between them (one-way ANOVA followed by *post-hoc* test; BST vs. ACo: $P=0.198$; BST vs. MeA: $P<0.001$; BST vs. PMCo: $P<0.001$; ACo vs. MeA: $P<0.001$; ACo vs. PMCo: $P<0.001$; MeA vs. PMCo, $P=0.375$) (Figure 1I).

AOB projects to BST and PMCo simultaneously

To test the features of the efferent axonal fibers of the AOB in mice, we used rAAV2-retro with different fluorescent protein elements, which do not repel each, to infect the same neurons (Zhu et al., 2019). Specifically, rAAV2-retro-Ef1α-EYFP-WPRE-pA and rAAV2-retro-Ef1α-mCherry-WPRE-pA were injected into two different accessory olfactory cortices simultaneously to achieve retrograde co-labeling of the AOB.

We first injected rAAV2-retro-Ef1α-EYFP-WPRE-pA into the BST (Figure 2B) and rAAV2-retro-Ef1α-mCherry-WPRE-pA into the PMCo (Figure 2C). The two kinds of rAAV2-retro showed overlapping into the MiA after four weeks (Figure 2D–F). We found that the percentage of co-labeled neurons in the MiA among all labeled neurons was higher in BST labeling than in PMCo labeling (BST vs. PMCo: 40.539%±6.850% vs. 5.80%±1.709%; one-way ANOVA, $F=24.219$, $P<0.001$, $n=3$) (Figure 2G). In addition, fluorescent markers of different colors appeared at both injection sites (not shown), indicating mutual regulation between the BST and PMCo.

AOB projects to ACo and PMCo simultaneously

In addition, we injected rAAV2-retro-Ef1α-EYFP-WPRE-pA into the ACo (Figure 3B) and rAAV2-retro-Ef1α-mCherry-WPRE-pA into the PMCo (Figure 3C). The two kinds of rAAV2-retro demonstrated overlapping in the MiA after four weeks (Figure 3D–F). We found that the percentage of co-labeled neurons in the MiA among all labeled neurons was greater in ACo labeling than in PMCo labeling (ACo vs. PMCo: 63.792%±4.578% vs. 19.758%±3.142%; one-way ANOVA, $F=62.882$, $P<0.001$, $n=3$) (Figure 3G). In addition, fluorescent markers of different colors appeared at both injection sites (Figure 3B, C), indicating mutual regulation between the ACo and PMCo.

AOB projects to PMCo and MeA simultaneously

We injected rAAV2-retro-Ef1α-mCherry-WPRE-pA into the MeA (Figure 4B) and rAAV2-retro-Ef1α-EYFP-WPRE-pA into

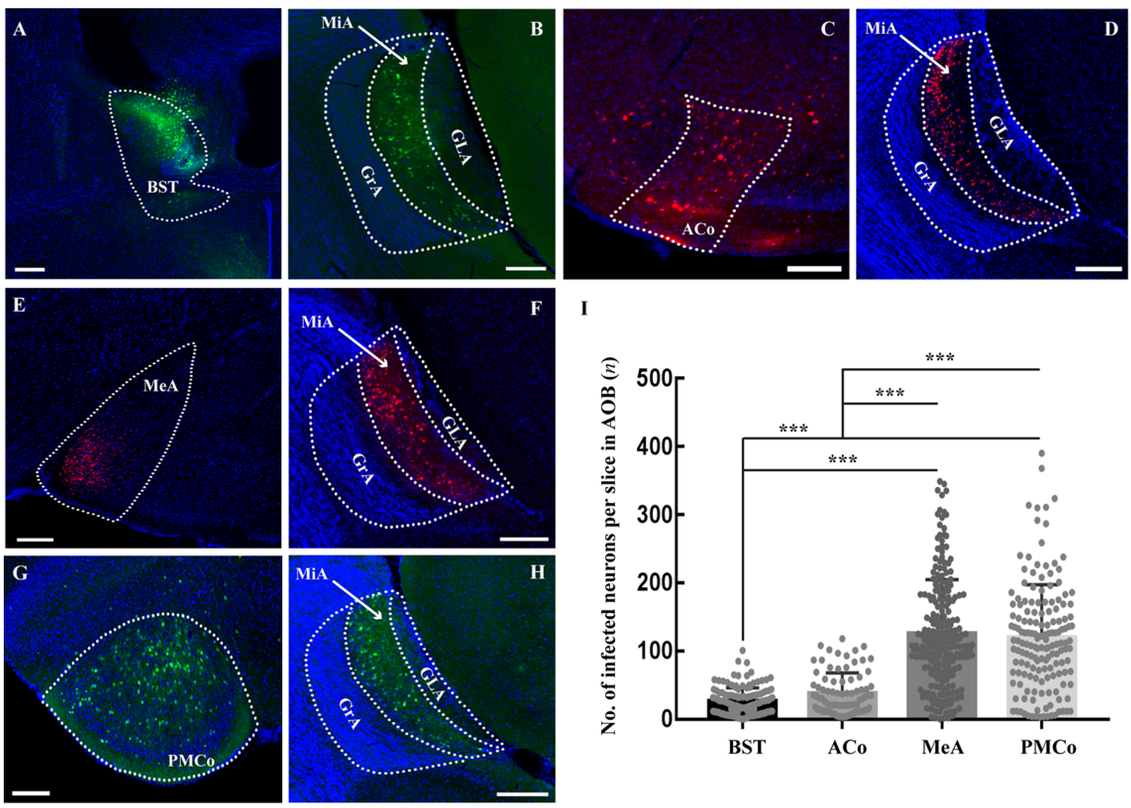

Figure 1 Mitral cell layer of AOB (MiA) projecting to BST, ACo, MeA, and PMCo

A, B: BST was injected with rAAV2-retro-Ef1α-EYFP-WPRE-pA (in green) (A) and MiA was labeled after four weeks (B). C, D: ACo was injected with rAAV2-retro-Ef1α-mCherry-WPRE-pA (in red) (C) and MiA was labeled after four weeks (D). E, F: MeA was injected with rAAV2-retro-Ef1α-mCherry-WPRE-pA (in red) (E) and MiA was labeled after four weeks (F). G, H: PMCo was injected with rAAV2-retro-Ef1α-EYFP-WPRE-pA (in green) (G) and MiA was labeled after four weeks (H). I: No. of infected neurons in MiA per slice varied in different retrograde-labeled brain regions. ***: P<0.001. Scale bars: 200 μm. n=10, 6, 16, 11.

the PMCo (Figure 4C). The two kinds of rAAV2-retro showed overlapping in the MiA after four weeks (Figure 4D–F). We found that the percentage of co-labeled neurons in the MiA among all labeled neurons was higher in PMCo labeling than in MeA labeling (PMCo vs. MeA: 95.836%±0.763% vs. 34.954%±2.494%; one-way ANOVA, F=544.944, P<0.001, n=3) (Figure 4G). In addition, fluorescent markers of different colors appeared at both injection sites (Figure 4B, C), indicating mutual regulation between the PMCo and MeA.

AOB projects to BST and MeA simultaneously

We injected rAAV2-retro-Ef1α-EYFP-WPRE-pA into the BST (Figure 5B) and rAAV2-retro-Ef1α-mCherry-WPRE-pA into the MeA (Figure 5C). The two kinds of rAAV2-retro showed overlapping in the MiA after four weeks (Figure 5D–F). We found that the percentage of co-labeled neurons in the MiA among all labeled neurons was greater in BST labeling than in MeA labeling (BST vs. MeA: 70.645%±3.288% vs. 13.888%±0.848%; one-way ANOVA, F=284.577, P<0.001, n=3) (Figure 5G). In addition, fluorescent markers of different colors appeared at both injection sites (Figure 5B, C), indicating mutual regulation between the BST and MeA.

AOB projects to ACo and MeA simultaneously

We injected rAAV2-retro-Ef1α-EYFP-WPRE-pA into the ACo (Figure 6B) and rAAV2-retro-Ef1α-mCherry-WPRE-pA into the MeA (Figure 6C). The two kinds of rAAV2-retro demonstrated overlapping in the MiA after four weeks (Figure 6D–F). We found that the percentage of co-labeled neurons in the MiA among all labeled neurons was greater in MeA labeling than in ACo labeling (ACo vs. MeA: 38.538%±2.460% vs. 15.685%±2.531%; one-way ANOVA, F=41.919, P<0.001, n=3) (Figure 6G). In addition, green fluorescent markers appeared at the MeA (Figure 6C), indicating projections from the MeA to ACo. Red fluorescent markers were found at the ACo (not shown), indicating mutual regulation between the ACo and MeA.

DISCUSSION

We used rAAV2-retro to successfully label AOB projection neurons in the MiA from the BST, ACo, MeA, and PMCo, and further adopted two-color rAAV2-retro to achieve co-labeling of mitral cells in the AOB. We demonstrated that a single neuron in the MiA could project to at least two different brain

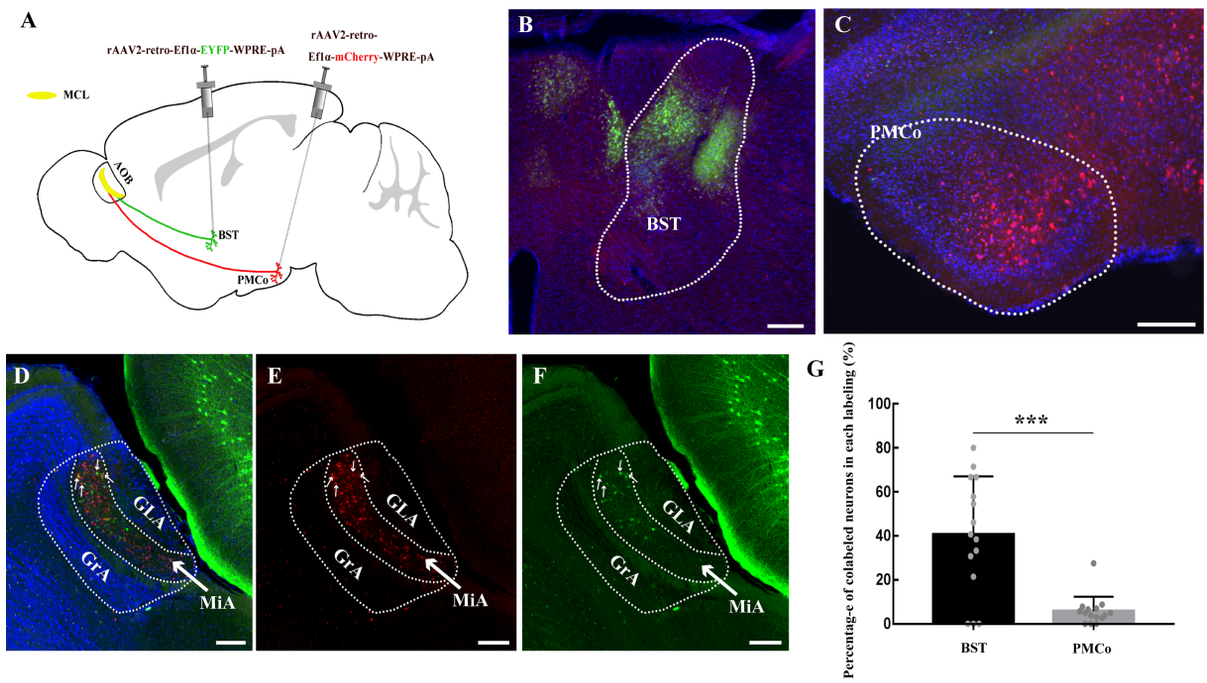

Figure 2 MiA projecting into BST and PMCo simultaneously

A: Schematic. B: Injection site of rAAV2-retro-Ef1α-EYFP-WPRE-pA (in green) in BST. C: Injection site of rAAV2-retro-Ef1α-mCherry-WPRE-pA (in red) in PMCo. D–F: Two kinds of rAAV2-retro overlapped in MiA after four weeks (arrows indicate co-labeled neurons). G: Percentages of co-labeled neurons in MiA among all labeled neurons in BST and PMCo labeling, respectively. ***: P<0.001. Scale bars: 200 μm. n=3.

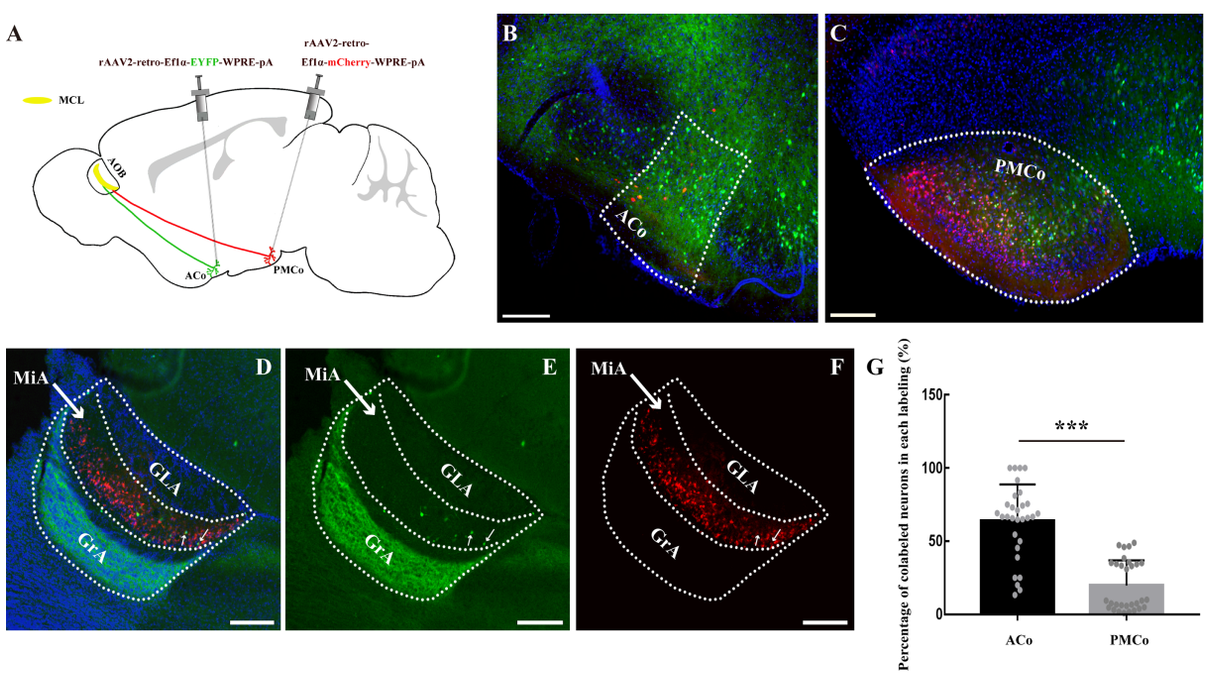

Figure 3 MiA projecting into ACo and PMCo simultaneously

A: Schematic. B: Injection site of rAAV2-retro-Ef1α-EYFP-WPRE-pA (in green) in ACo. C: Injection site of rAAV2-retro-Ef1α-mCherry-WPRE-pA (in red) in PMCo. D–F: Two kinds of rAAV2-retro overlapped in MiA after four weeks (arrows indicate co-labeled neurons). G: Percentages of co-labeled neurons in MiA among all labeled neurons in ACo and PMCo labeling, respectively. ***: P<0.001. Scale bars: 200 μm. n=3.

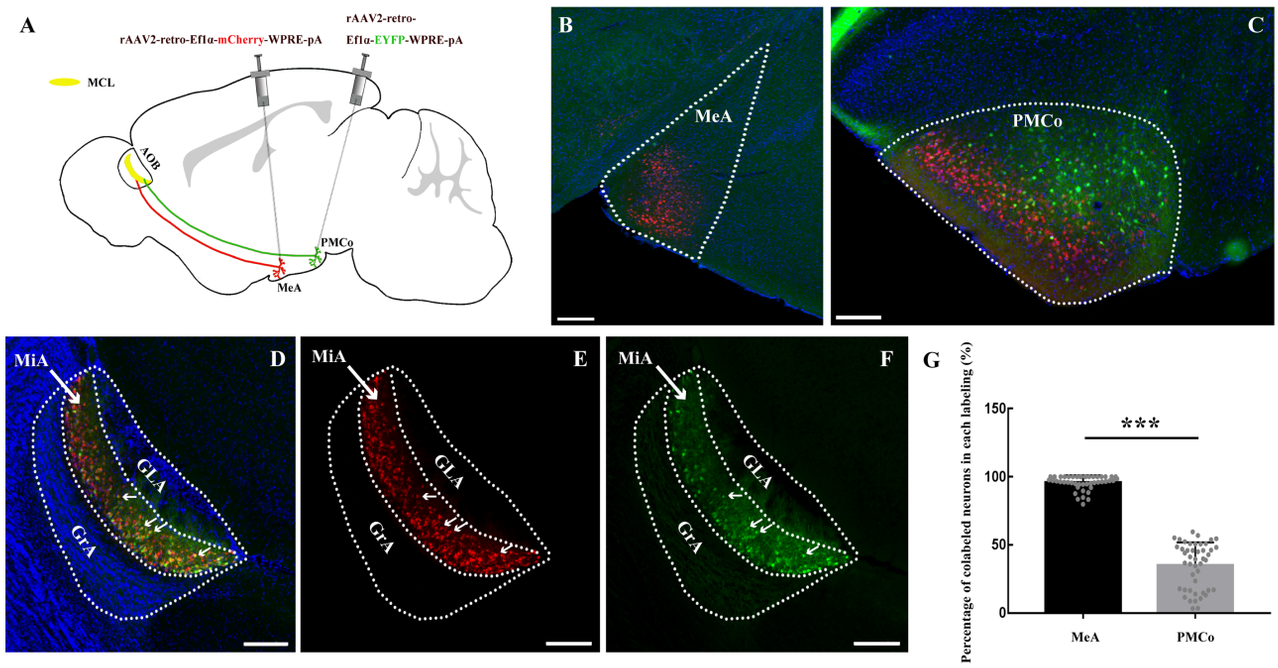

Figure 4 MiA projecting into PMCo and MeA simultaneously

A: Schematic. B: Injection site of rAAV2-retro-Ef1α-mCherry-WPRE-pA (in red) in MeA. C: Injection site of rAAV2-retro-Ef1α-EYFP-WPRE-pA (in green) in PMCo. D–F: Two kinds of rAAV2-retro overlapped in MiA after four weeks (arrows indicate co-labeled neurons). G: Percentages of co-labeled neurons in MiA among all labeled neurons from MeA and PMCo, respectively. ***: P<0.001. Scale bars: 200 μm. n=3.

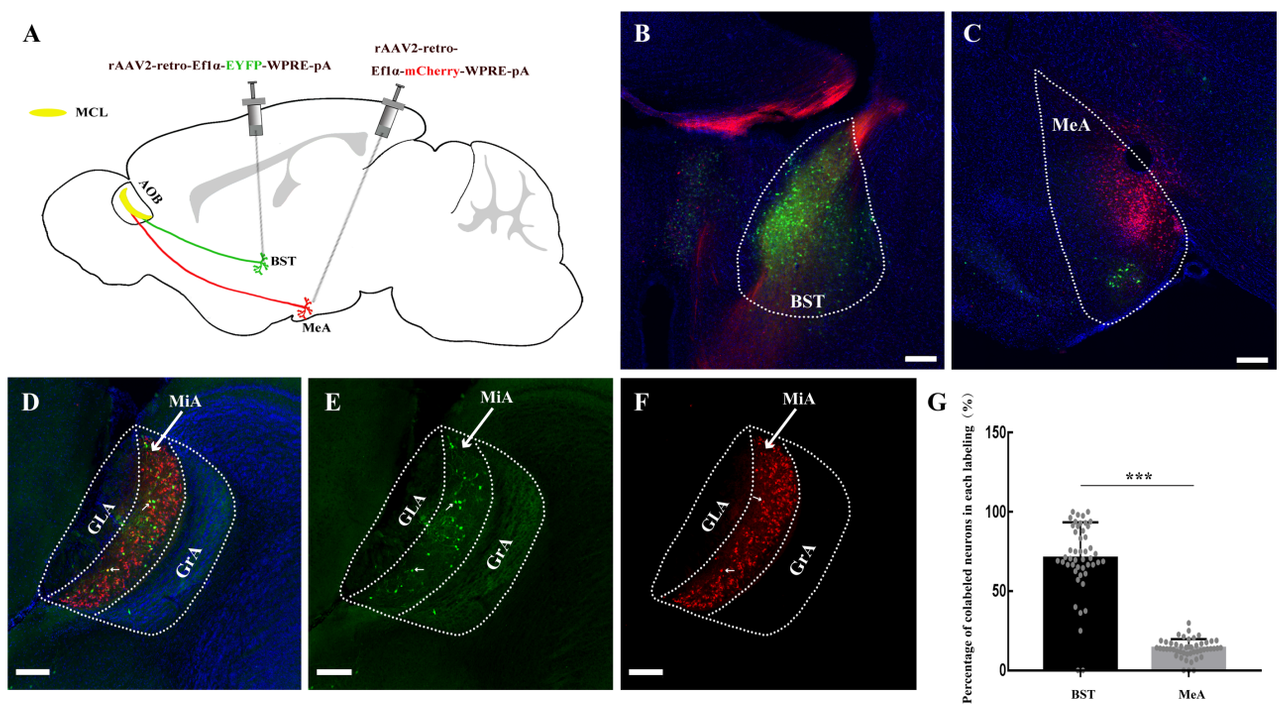

Figure 5 MiA projecting into BST and MeA simultaneously

A: Schematic. B: Injection site of rAAV2-retro-Ef1α-EYFP-WPRE-pA (in green) in BST. C: Injection site of rAAV2-retro-Ef1α-mCherry-WPRE-pA (in red) in MeA. D–F: Two kinds of rAAV2-retro overlapped in MiA after four weeks (arrows indicate co-labeled neurons). G: Percentages of co-labeled neurons in MiA among all labeled neurons from BST and MeA, respectively. ***: P<0.001. Scale bars: 200 μm. n=3.

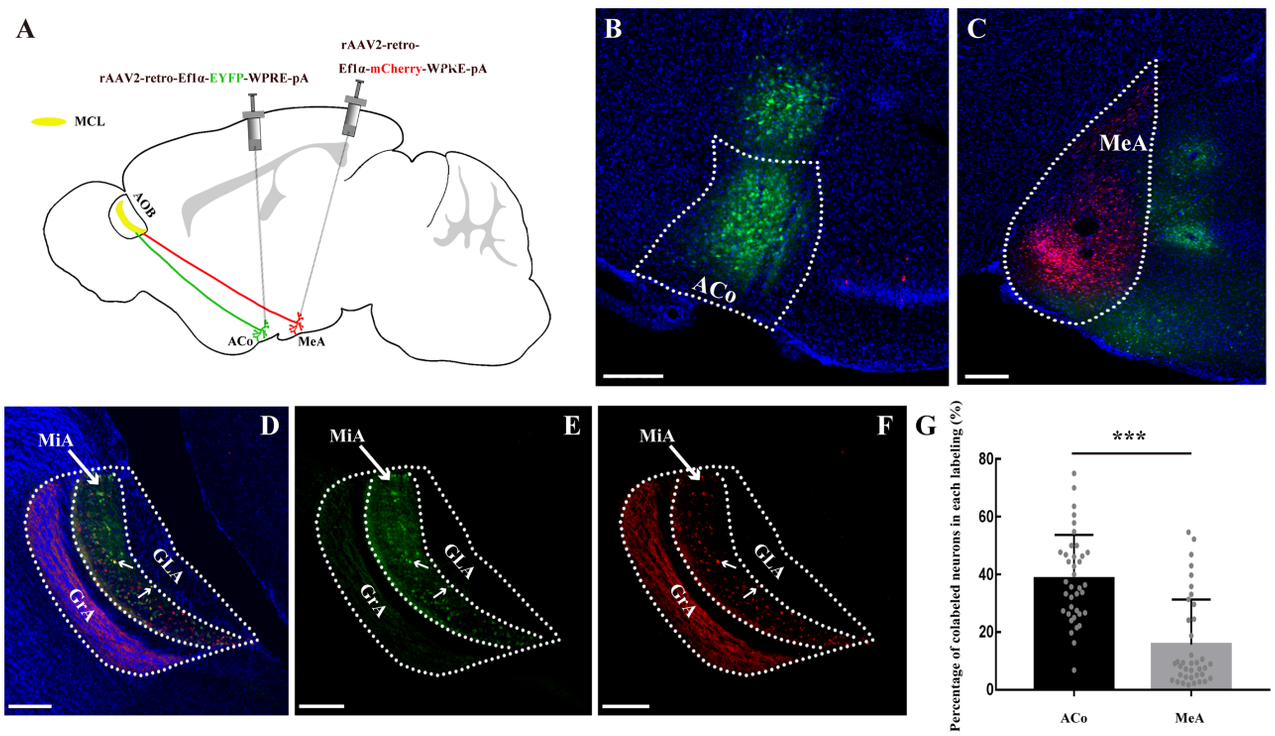

Figure 6 MiA projecting into ACo and MeA simultaneously

A: Schematic. B: Injection site of rAAV2-retro-Ef1α-EYFP-WPRE-pA (in green) in ACo. C: Injection site of rAAV2-retro-Ef1α-mCherry-WPRE-pA (in red) in MeA. D–F: Two kinds of rAAV2-retro overlapped in the MiA after four weeks (arrows indicate co-labeled neurons). G: Percentages of co-labeled neurons in MiA among all labeled neurons from ACo and MeA, respectively. ***: P<0.001. Scale bars: 200 μm. n=3.

regions. These results indicate that the dispersion characteristics of efferent projections of mitral cells in the AOB are similar to those of the MOB, that is, the axonal branches of individual mitral cells can reach all olfactory cortices (Nagayama et al., 2010). Although the dendrites, shapes, locations, and spontaneous and stimulus-induced activities of the AOB projection neurons rarely resemble those of MOB mitral cells (Larriva-Sahd, 2008; Mohrhardt et al., 2018), their transport patterns of information in the MOB and AOB may be similar, and different olfactory cortices may have different odor decoding mechanisms, eventually leading to different perceptions of odorants and pheromones.

We also found that the numbers of labeled neurons in the AOB from various cortices were significantly different, in the order BST<ACo<MeA<PMCo (Figure 1I). In addition, the percentages of co-labeled neurons from two cortices were highest in the BST, followed by the ACo and PMCo, and lowest in the MeA (Figures 2G, 3G, 4G, 5G, 6G), indicating that the number of labeled neurons in the AOB, from small to large, was in the order: BST, ACo, PMCo, and MeA. These results demonstrate that there were quantitative differences in the number of mitral cells in the AOB projecting to diverse accessory olfactory cortices, if the magnitude of the local axon terminals was the same in the rAAV-infected areas. However, given that rAAVs do not fully infect the entire targeted brain region, the number of labeled neurons in the AOB was incomplete. According to previous results, a single AOB harbors 6 842 putative mitral cells (Mohrhardt et al., 2018), which is 4–18 times greater than that labeled in our study (Figure 1I, MeA: 111.06±74.39, PMCo: 117.12±82.213, BST: 26.05±20.061, ACo: 48.3±36.943; approximately 15 slices in one AOB). Therefore, we cannot conclude that there are differences in the number of neurons in the AOB projecting into different brain regions. However, there may be significant differences in the number of neurons projecting to the same area in different brain regions, suggesting that each mitral cell in the AOB could project to a different number of neurons in different cortices, but this requires more sophisticated single-cell markers for detection and validation.

In addition, we found that there was no significant difference in the projection pattern between the aAOB and pAOB, although their sources of input are isolated from each other (Dulac & Torello, 2003; Riviere et al., 2009). Nevertheless, only the aAOB or pAOB showed retrograde labeling, but limitedly (Figure 2F, form BST; Figure 3E, form ACo). These results are similar to previous research, which used anterograde and retrograde chemical tract-tracing methods in rats and demonstrated that apart from common vomeronasal-recipient areas, only the aAOB projects to the BST, medial division, and posteromedial part (BSTMPM), and only the pAOB projects to the dorsal anterior amygdale (AAd), deep cell layers of the bed nucleus of the accessory olfactory tract

(BAOT), and anteroventral MeA (MeAV) (Mohedano-Moriano et al., 2007). The midline separating the aAOB and pAOB is determined by the boundary of Gαi2 labeling between the anterior and posterior glomerular layer (GLA), which is roughly perpendicular to the AOB (Marking et al., 2017). Because of the larger local diffusion range of rAAVs, we cannot suggest significant anatomical and functional differences between the aAOB and pAOB, but their axonal projection patterns have a certain degree of convergence (von Campenhausen & Mori, 2000).

Finally, we found reciprocal projections between cortices, such as the ACo and PMCo (Figure 3B, C), MeA and PMCo (Figure 4B, C), MeA and BST (Figure 5B, C), and MeA and ACo (Figure 6B, C), which suggests that these brain regions regulate each other. Combined with previous results, these findings indicate that the way in which information is decoded in the accessory olfactory cortex remains unknown. Moreover, we found that no neurons in the MOB were labeled from the above-mentioned accessory olfactory cortices, including the CoA and MeA, which have been reported to receive inputs from the MOB (Kang et al., 2009). Whether the information convergence point of the MOS and AOS is the hypothalamus or the cortical amygdala (Kang et al., 2009; Perez-Gomez et al., 2015), or even direct connections between the MOB and AOB at the very beginning (Vargas-Barroso et al., 2015), is still controversial, requiring additional experiments with more sophisticated single-cell labeling tools to enable verification.

Our study provides an effective method for labeling mitral cells in the AOB of mice and demonstrated that their axonal projection pattern was the same as in the MOB, i.e., dispersion characteristics of efferent projections to each cortex through a large number of axonal branches. Moreover, we found no significant differences between the aAOB and pAOB in projections to the BST, ACo, MeA, and PMCo, although their inputs were distinguishable from the apical and basal VNO (Figure 7). Further single-cell labeling and recordings are necessary to elucidate the projection patterns and information encoding of individual mitral cells in the aAOB and pAOB and whether individual cortical neurons sample information across segregated AOB pathways. It would be useful to study what pheromone information is represented in the different accessory olfactory cortices and to understand how the brain processes pheromone signals to elicit stereotypical behavioral responses.

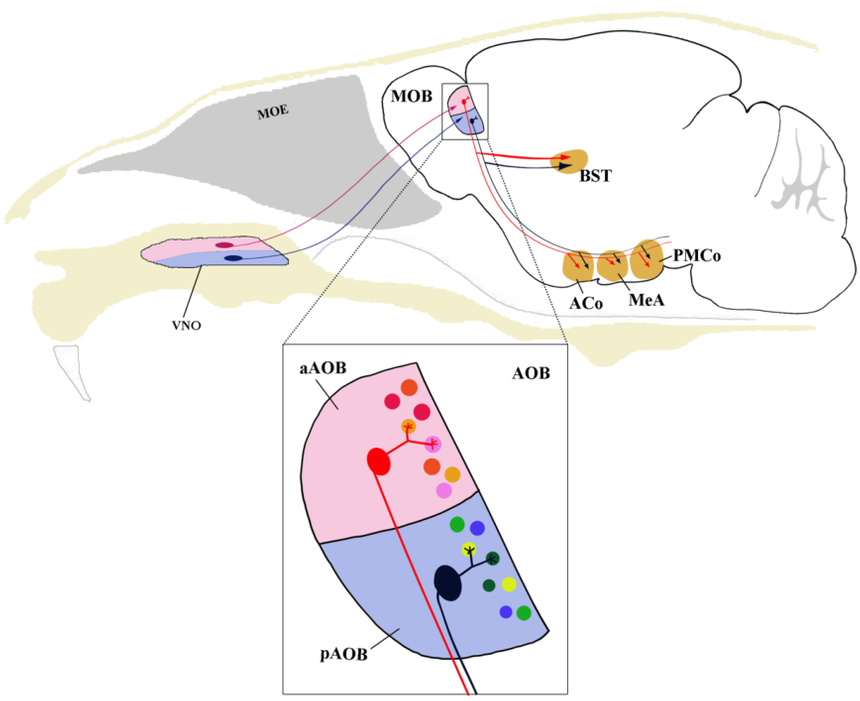

Figure 7 Schematic of afferent projections in accessory olfactory system of mice

COMPETING INTERESTS

The authors declare that they have no competing interests.

AUTHORS' CONTRIBUTIONS

X.P.R., X.T.Z, and F.Q.X. designed the study. N.Z. and X.P.R. supervised the analyses. N.Z., Z.Z.W., S.W.W., F.J.Y., C.L., and X.P.R. performed labeling and statistics. N.Z. and X.P.R wrote the manuscript with the other authors' input. A.M. polished the manuscript. N.Z and X.P.R revised the manuscript. All authors read and approved the final version of the manuscript.

ACKNOWLEDGEMENTS

We thank Dr. Ling-Ling Xu (Wuhan Institute of Physics and Mathematics) for maintaining and managing the optical platform.

REFERENCES

Ackels T, Drose DR, Spehr M. 2016. In-depth physiological analysis of defined cell populations in acute tissue slices of the mouse vomeronasal organ. *Journal Visuallized Experiments*.

Breer H, Fleischer J, Strotmann J. 2006. The sense of smell: multiple olfactory subsystems. *Cellular and Molecular Life Sciences CMLS*, **63**: 1465−1475.

Doving KB, Trotier D. 1998. Structure and function of the vomeronasal organ. *Journal Experimental Biologyl*, **201**: 2913−2925.

Dulac C, Torello AT. 2003. Molecular detection of pheromone signals in mammals: from genes to behaviour. *Nature Reviews Neuroscience*, **4**: 551−562.

Dulac C, Wagner S. 2006. Genetic analysis of brain circuits underlying pheromone signaling. *Annual Review of Genetics*, **40**: 449−467.

Ghosh S, Larson SD, Hefzi H, Marnoy Z, Cutforth T, Dokka K, Baldwin KK. 2011. Sensory maps in the olfactory cortex defined by long-range viral tracing of single neurons. *Nature*, **472**: 217−220.

Halpern M, Martinez-Marcos A. 2003. Structure and function of the vomeronasal system: an update. *Progress in Neurobiology*, **70**(3): 245−318.

Holy TE. 2018. The accessory olfactory system: Innately specialized or microcosm of mammalian circuitry?. *Annual review of neuroscience*, **41**: 501−525.

Kang N, Baum MJ, Cherry JA. 2009. A direct main olfactory bulb projection to the 'vomeronasal' amygdala in female mice selectively responds to volatile pheromones from males. *The European Journal of Neuroscience*, **29**(3): 624−634.

Krieger J, Schmitt A, Lobel D, Gudermann T, Schultz G, Breer H, Boekhoff I. 1999. Selective activation of G protein subtypes in the vomeronasal organ upon stimulation with urine-derived compounds. *The Journal of Biological Chemistry*, **274**(8): 4655−4662.

Larriva-Sahd J. 2008. The accessory olfactory bulb in the adult rat: a cytological study of its cell types, neuropil, neuronal modules, and interactions with the main olfactory system. *The Journal of Comparative Neurology*, **510**(3): 309−350.

Leinders-Zufall T, Brennan P, Widmayer P, S PC, Maul-Pavicic A, Jager M, Li XH, Breer H, Zufall F, Boehm T. 2004. MHC class I peptides as chemosensory signals in the vomeronasal organ. *Science*, **306**(5698): 1033−1037.

Leinders-Zufall T, Lane AP, Puche AC, Ma W, Novotny MV, Shipley MT, Zufall F. 2000. Ultrasensitive pheromone detection by mammalian vomeronasal neurons. *Nature*, **405**: 792−796.

Marking S, Krosnowski K, Ogura T, Lin W. 2017. Dichotomous distribution of putative cholinergic interneurons in mouse accessory olfactory bulb. *Frontiers in Neuroanatomy*, **11**: 10.

Miyamichi K, Amat F, Moussavi F, Wang C, Wickersham I, Wall NR, Taniguchi H, Tasic B, Huang ZJ, He Z, Callaway EM, Horowitz MA, Luo L. 2011. Cortical representations of olfactory input by trans-synaptic tracing. *Nature*, **472**: 191−196.

Mohedano-Moriano A, Pro-Sistiaga P, Ubeda-Banon I, Crespo C, Insausti R, Martinez-Marcos A. 2007. Segregated pathways to the vomeronasal amygdala: differential projections from the anterior and posterior divisions of the accessory olfactory bulb. *The European Journal of Neuroscience*, **25**(7): 2065−2080.

Mohrhardt J, Nagel M, Fleck D, Ben-Shaul Y, Spehr M. 2018. Signal detection and coding in the accessory olfactory system. *Chemical Senses*, **43**(9): 667−695.

Moriya-Ito K, Endoh K, Fujiwara-Tsukamoto Y, Ichikawa M. 2013. Three-dimensional reconstruction of electron micrographs reveals intrabulbar circuit differences between accessory and main olfactory bulbs. *Frontiers in Neuroanatomy*, **7**: 5.

Nagayama S, Enerva A, Fletcher ML, Masurkar AV, Igarashi KM, Mori K, Chen WR. 2010. Differential axonal projection of mitral and tufted cells in the mouse main olfactory system. *Frontiers in Neural Circuits*, **4**: 120.

Perez-Gomez A, Bleymehl K, Stein B, Pyrski M, Birnbaumer L, Munger SD, Leinders-Zufall T, Zufall F, Chamero P. 2015. Innate predator odor aversion driven by parallel olfactory subsystems that converge in the ventromedial hypothalamus. *Current Biology*, **25**(10): 1340−1346.

Riviere S, Challet L, Fluegge D, Spehr M, Rodriguez I. 2009. Formyl peptide receptor-like proteins are a novel family of vomeronasal chemosensors. *Nature*, **459**: 574−577.

Sosulski DL, Bloom ML, Cutforth T, Axel R, Datta SR. 2011. Distinct representations of olfactory information in different cortical centres. *Nature*, **472**: 213−216.

Spehr M, Spehr J, Ukhanov K, Kelliher KR, Leinders-Zufall T, Zufall F. 2006. Parallel processing of social signals by the mammalian main and accessory olfactory systems. *Cellular Molecular Life Sciences*, **63**: 1476−1484.

Su CY, Menuz K, Carlson JR. 2009. Olfactory perception: receptors, cells, and circuits. *Cell*, **139**: 45−59.

Takami S, Graziadei PP. 1991. Light microscopic Golgi study of mitral/tufted cells in the accessory olfactory bulb of the adult rat. *The Journal of Comparative Neurology*, **311**(1): 65−83.

Urban NN, Castro JB. 2005. Tuft calcium spikes in accessory olfactory bulb mitral cells. *The Journal of Neuroscience: the Official Journal of the Society for Neuroscience*, **25**(20): 5024−5028.

Vargas-Barroso V, Ordaz-Sanchez B, Pena-Ortega F, Larriva-Sahd JA. 2015. Electrophysiological evidence for a direct link between the main and accessory olfactory bulbs in the adult rat. *Frontiers in Neuroscience*, **9**: 518.

von Campenhausen H, Mori K. 2000. Convergence of segregated pheromonal pathways from the accessory olfactory bulb to the cortex in the mouse. *The European Journal of Neuroscience*, **12**(1): 33−46.

Yokosuka M. 2012. Histological properties of the glomerular layer in the mouse accessory olfactory bulb. *Experimental Animals*, **61**(1): 13−24.

Yoles-Frenkel M, Kahan A, Ben-Shaul Y. 2018. Temporal response properties of accessory olfactory bulb neurons: limitations and opportunities for decoding. *The Journal of Neuroscience: the Official Journal of the Society for Neuroscience*, **38**(21): 4957−4976.

Yonekura J, Yokoi M. 2008. Conditional genetic labeling of mitral cells of the mouse accessory olfactory bulb to visualize the organization of their apical dendritic tufts. *Molecular and Cellular Neuroscience*, **37**(4): 708−718.

Zhu X, Lin K, Liu Q, Yue X, Mi H, Huang X, He X, Wu R, Zheng D, Wei D, Jia L, Wang W, Manyande A, Wand J, Zhang Z, Xu F. 2019. Rabies virus pseudotyped with CVS-N2C glycoprotein as a powerful tool for retrograde neuronal network tracing. *Neuroscience Bulletin*.